chemosensors

Article

A Sensor for Electrochemical pH Monitoring Based on Laser-Induced Graphene Modified with Polyfolate

Vytautas Žutautas [1], Romualdas Trusovas [2], Aivaras Sartanavičius [2], Karolis Ratautas [2], Algirdas Selskis [3] and Rasa Pauliukaite [1,*]

[1] Department of Nanoengineering, Center for Physical Sciences and Technology, Savanoriu Ave. 231, LT-02300 Vilnius, Lithuania
[2] Department of Laser Technologies, Center for Physical Sciences and Technology, Savanoriu Ave. 231, LT-02300 Vilnius, Lithuania
[3] Department of Characterisation of Materials Structure, Center for Physical Sciences and Technology, Saulėtekio Ave. 3, LT-10257 Vilnius, Lithuania
* Correspondence: rasa.pauliukaite@ftmc.lt

Abstract: A laser-induced graphene (LIG) modified with chitosan (Chit) and conducting polymer polyfolate (PFA) was used as a base to develop a flat and flexible pH sensor. LIGs were formed using two different irradiation wavelengths of 355 nm and 532 nm. Depending on the wavelengths, the obtained electrodes were named LIG355 and LIG532. Microscopic imaging revealed that the bare LIG electrode surface had rough structures after laser treatment giving hydrophilic properties, and that PFA forms fibre-like structures on Chit coated LIG. Electrochemical investigation with the redox probe demonstrated that diffusion is a limiting process at the bare and modified LIG electrodes. A capacitive behaviour was observed from electrochemical impedance spectra at bare electrodes, showing a rather rough interface at LIG355 but a microporous one at LIG532. The developed flat and flexible electrode was sensitive to pH in the region from 6.0 to 9.0. In the studied pH range, the sensitivity was 27.86 ± 0.81 for PFA/Chit/LIG355 and 30.32 ± 0.50 mV/pH for PFA/Chit/LIG532 with moderate stability for a period of more than two months.

Keywords: pH monitoring; polyfolate; potentiometry; electrochemistry; electrochemical sensor; chitosan; laser-inducted graphene electrode

Citation: Žutautas, V.; Trusovas, R.; Sartanavičius, A.; Ratautas, K.; Selskis, A.; Pauliukaite, R. A Sensor for Electrochemical pH Monitoring Based on Laser-Induced Graphene Modified with Polyfolate. *Chemosensors* **2023**, *11*, 329. https://doi.org/10.3390/chemosensors11060329

Academic Editors: Manel del Valle and Núria Serrano

Received: 11 April 2023
Revised: 19 May 2023
Accepted: 1 June 2023
Published: 2 June 2023

1. Introduction

Laser-induced graphene (LIG) is a carbon-based nanomaterial that is fabricated in a single step by applying laser irradiation to various carbon-containing materials [1]. It is easily applicable and scalable as a wide range of lasers—from CO_2 [2,3] to pulsed lasers [4–7], and it can be combined with various materials such as wood [8], textile [6], paper [9], or thermoplastics [10].

The advantage of this method is that LIG formation usually does not involve using hazardous chemical materials and does not require high vacuum or complex thermal management such as chemical vapour deposition (CVD). Therefore, due to the nature of some precursors, LIG-based electronic devices are strong candidates for sustainability and the circular economy. Furthermore, LIG has been applied to various materials by different research groups using various laser sources such as pulsed 1064 nm, 532 nm, and 355 nm lasers, as well as CO_2 lasers. When using pulsed lasers and shorter wavelengths, the photochemical effect dominates during LIG formation as the high-energy photons directly excite precursor material molecules, leading to the breakage of chemical bonds. In contrast, CO_2 laser irradiation promotes the photothermal effect, producing thermal energy that causes lattice vibrations and breaks chemical bonds [11–13]. Laser-activated graphene is a conductor; in such a way, LIG allows forming of conductive areas on insulating substrates, which leads to the production of devices such as supercapacitors [4,14,15], strain sensors [9],

pH sensors [16], and antennas [17]. Since LIG can also be formed on thin, flexible films, it is helpful for developing flexible wearable electronics [6,18]. Furthermore, as LIG surfaces possess antiviral and antibacterial properties, this material can be applied for air/water filtering or the production of antiviral surfaces [1].

Polyfolate (PFA) is a conductive polymer formed from electrochemically polymerised folate monomer, which is a deprotonated folic acid form. Polymerisation mechanisms were studied in previous work [19]. It was noticed that the deposition solution and its pH influence PFA formation on the electrode and its surface morphology. FA is also sensitive to a pH range between 6.0 and 10.0 [20]. Moreover, PFA was previously used to develop sensors for glucose [21], dopamine [22], and pH [23].

A pH sensor is a system that determines proton concentration and its change. It is necessary because many chemical processes depend on pH. Although buffer solutions can be used to keep constant pH, sometimes pH can change in different steps of the process. In the literature, several pH sensor types are reported, including optical fibre, mass-sensitive, metal oxide, nano-constructed cantilever, ion-selective field-effect transistor (ISFET), capacitive, colourimetric, and conducting polymer-based pH sensors [24–29]. The most popular and widely used pH sensor is a glass electrode that was first reported more than a century ago by Max Cremer [30]. However, glass electrodes require calibration, and it is difficult to use them in minimised and flexible systems. Therefore, it is necessary to create a flat and flexible sensor that can be easily minimised. For this, pH-dependent conductive polymers [31] can be adapted.

In this work, LIG and PFA were used to create flexible pH sensors that do not require constant calibration. For this, bare and modified with PFA LIG electrodes were characterised using microscopic, spectroscopic, and electrochemical techniques. As a possible application, the potentiometric response to pH at the PFA/LIG electrode was investigated. To improve the stability of the electrode, before PFA polymerisation, the LIG was coated with chitosan (Chit), and the conditions of the electrode modification were optimised. The resulting sensor was further characterised and its response to pH between 6.0 and 9.0 was tested using potentiometry.

2. Materials and Methods

2.1. Chemicals and Solutions

FA, KCl, NaCl, $K_4[Fe(CN)_6]\cdot 3H_2O$, and Chit were obtained from Sigma Aldrich (Taufkirchen, Germany). $NaH_2PO_4\cdot H_2O$, Na_2HPO_4, NaOH, and HCl were obtained from ROTH GmbH (Karlsruhe, Germany). All reagents used were of analytical grade and used as received.

The aqueous solutions were prepared in ultrapure Milli-Q water (resistivity of 18.2 MWcm) taken from the Synergy 185 unit with the UV lamp (Millipore, Burlington, MA, USA).

For electrochemical experiments, 0.1 M sodium phosphate buffer saline with 0.15 M NaCl (PBS), pH 6.00 ± 0.04, 7.00 ± 0.08, 8.00 ± 0.05, and 9.00 ± 0.05, was used as the supporting electrolyte. In some cases, the supporting electrolyte was 0.1 M KCl with the addition of 0.01 M HCl, pH 2.00 ± 0.04.

Polyimide Kapton® films from DuPont (Wilmington, DE, USA) with a thickness of 127 µm were used in our experiments.

2.2. Methods

A picosecond laser Atlantic (Ekspla, Lithuania) was used for LIG formation. Galvoscanners SCANcube and hurrySCAN (Scanlab, Germany) were used for laser beam scanning. An Olympus BX51 upright fluorescence microscope (Olympus, Tokyo, Japan) equipped with air and water immersion objectives and an F-View II Peltier-cooled CCD camera was used to acquire optical microscopy images. The images were obtained using Stream motion software (Olympus, Germany), and the analysis was performed using ImageJ's public domain image processing program. Brightfield images were obtained in the air.

The scanning electron microscopes Helios NanoLab 650 (FEI) and JSM-6490 LV (JEOL) were used to investigate surface morphology changes during laser treatment of the polyimide (PI) sample. Samples were used without any additional preparation in scanning electron microscopy (SEM) characterisation. Images were acquired with Helios NanoLAb 650 using 3–5 kV voltage and 1000–200,000× magnification, with JSM-6490 LV—7–10 kV voltage and 500–1000× magnification.

Raman spectroscopic measurements were performed with the Raman spectrometer/microscope in Via (Renishaw, UK) equipped with the thermoelectrically cooled (−70 °C) CCD detector. Spectra were excited with the 532 nm wavelength laser irradiation dispersed by 1800 grooves/mm grating. The spectra were taken using a 50×/0.75NA objective lens. Spectral peaks were fitted with the Voigt function using OriginPro 8.5 software from OriginLab Corporation, Northampton, MA, USA.

Wettability measurements were made using contact angle (CA) characterisation and were performed employing the optical contact angle measuring and contour analysis system (OCA 15EC, Data-Physics Instruments GmbH, Filderstadt, Germany) together with a CCD camera to capture lateral images of water droplets applied on flat, modified LIG electrodes. A droplet of deionised water with a volume of 1 µL for bare LIG and 3 µL for Chit and PFA/Chit modified electrodes was deposited using a syringe with a 1 mm diameter pipette (Fisnar QuantX™, Brand, Germantown, WI, USA). The illumination source with a light-emitting diode, the water droplet, and the camera were aligned into one line. Therefore, the digital camera captured the water droplet projection. Analysis was performed using KRÜSS ADVANCE software.

Potentiostat/galvanostat CompactStat (Ivium Technologies, Eindhoven, The Netherlands), assembled with the three-electrode system, was used for electrochemical investigations. Flat and flexible laser-induced graphene (LIG, 1.0 cm × 2.0 cm, LIG355 or LIG532) on PI substrate served as working electrodes. For the counter electrode, a Pt wire was used, and for the reference, an Ag/AgCl (sat. KCl) electrode was implemented. All potentials in this paper are given versus this reference.

Electrodes were characterised electrochemically by employing cyclic voltammetry (CV), PA, and electrochemical impedance spectroscopy (EIS). EIS was carried out at a constant applied potential at peak positions in a frequency range from 10 kHz to 100 mHz, with a potential perturbation of 10 mV. The EIS spectra were analysed with ZView software (Scribner Associates, Southern Pines, NC, USA).

The PH211 Microprocessor pH Meter from Hanna Instruments (Woonsocket, RI, USA) was used for the comparative pH measurements.

OriginPro 9 (OriginLab Corporation, Northampton, MA, USA) was employed to plot the resulting data.

2.3. Preparation of the LIG Electrodes

LIG was formed on a PI film (source) surface using the picosecond laser Atlantic (Ekspla, Vilnius, Lithuania). The laser pulse duration was 10 ps, the pulse repletion rate was 100 kHz, and the irradiation wavelengths were 355 nm and 532 nm. Galvosanners SCANcube (for 355 nm wavelength) from SANLAB (Lohmar, Germany) and hurrySCAN (for 532 nm wavelength) were used for beam control. Further in the text, these LIG samples are named LIG355 (processed with 355 nm) and LIG532 (processed with a 532 nm beam). The PI film was placed 4 mm above focus (355 nm) or in the focal plane (532 nm), and rectangular shapes (1.0 cm × 2.0 cm) were scanned using the laser beam (Figure 1). The laser processing parameters are shown in Table 1. These laser processing parameters were determined by irradiating PI with various laser process parameters and analysing LIG sheet resistance.

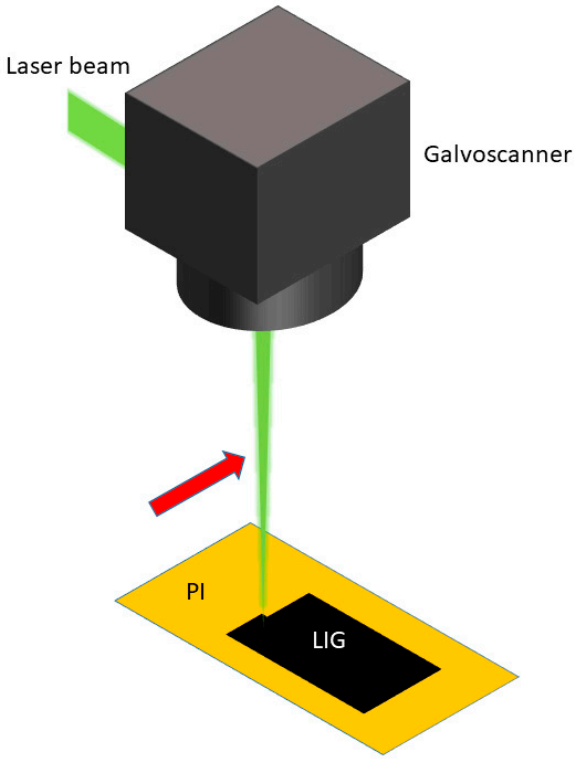

Figure 1. LIG formation with picosecond laser setup.

Table 1. Laser process parameters of LIG formation.

Sample	LIG355	LIG532
Wavelength, nm	355	532
Irradiation power, mW	200	500
Scanning speed, mm/s	10	50
Repeat times	5	5
Hatch, µm	10	10
Position regarding beam focus	4 mm above the focus	At the focus

Prior to modification, the LIG surface was rinsed with the Mili-Q water and dried with an N_2 stream. The experimental area used in electrochemical measurements was 1.0 × 0.5 cm. The remaining part was insulated with the chitosan coating, which was covered on top with Flormar Pearly Nail Enamel Pl 308 (Figure 2). Afterwards, the electrode was polished electrochemically in 0.1 M KCl by scanning the applied potential repeatedly between −1.0 V and +1.0 V at a scan rate of 200 mV s^{-1} for at least 20 cycles until constant voltammograms were obtained. To modify the electrode directly with PFA, it was successively rinsed with the deionised water and transferred to the electropolymerisation solution containing 0.1 M PBS, pH 6.0, with 1.0 mM FA. PFA was obtained using CV of the applied potential between −1.5 V and +1.7 V at the potential scan rate of 50 mV s^{-1} for 75 (with LIG355) and 72 (with LIG532) cycles.

In other cases, the 0.5 cm^2 experimental area was drop coated with 70 µL of 1% Chit solution in 1% acetic acid and air-dried for 1 day. Then, the electropolymerisation was carried out as described above and air-dried for 1 day, which yielded either PFA/Chit/LIG355 or PFA/Chit/LIG532.

For microscopic investigations, LIG electrodes were separated with the coating from chitosan and nail enamel into three sections of 0.5 cm^2 each: (i) left as bare LIG, (ii) coated with chitosan (Chit/LIG), and (iii) coated with chitosan and PFA (PFA/Chit/LIG).

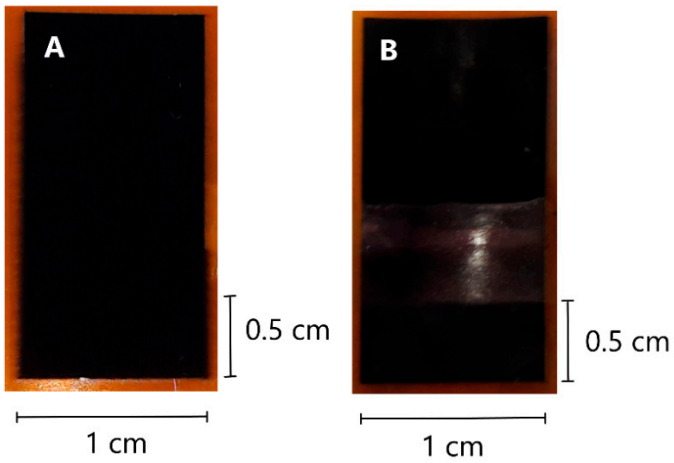

Figure 2. Photographs of 1.0 cm × 2.0 cm LIG electrodes. Bare LIG electrode (**A**) with chosen experimental area 1.0 cm × 0.5 cm and LIG with the experimental area insulated using chitosan coating with nail enamel (**B**).

3. Results

3.1. Characterisation of the LIG Electrode

The surface quality of the electrode was investigated by observing the topography with SEM. The LIG structure was investigated using Raman spectroscopy, and electrochemical behaviour was studied using CV and EIS.

The surface morphology investigation of both LIG samples is presented in Figure 3. Periodical structures formed by scanning PI surfaces with a focused pulsed laser beam were observed on both electrodes. The laser irradiation forms a rough surface by breaking chemical bonds in PI molecules. As seen, the flake-like structures are apparent in both samples. In the case of LIG355, the surface appears to be disrupted by laser irradiation, and the flake distribution is uneven. Moreover, the variation of the flake size is more visible in comparison to the LIG532 surface. The formation of a layered graphite-like structure of the LIG532 sample is observed with a larger magnification (Figure 3C,D).

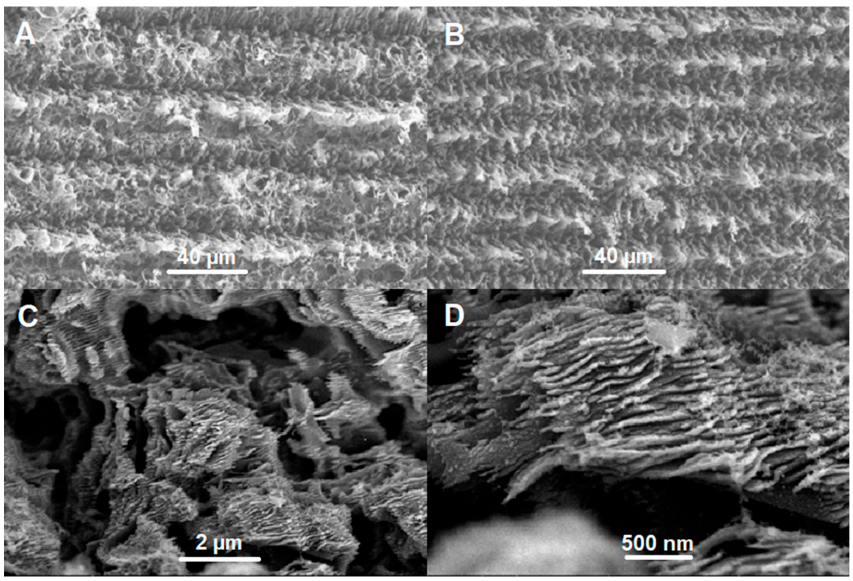

Figure 3. SEM 1000× images of LIG355 (**A**), LIG532 (**B**), and images of different magnifications of LIG532: 20,000× (**C**), 65,047× (**D**).

Further, the study of the LIG structure was performed with Raman spectroscopy, one of the best tools for characterising carbonaceous nanomaterials. The Raman spectra of

LIG355 and LIG532 are presented in Figure 4. The spectra of both samples show prominent peaks, which are characteristic of multilayer graphene. Furthermore, both spectra show a similar intensity, close to the 1 I(D)/I(G) ratio, confirming identical point-like defects in both materials. A more thorough analysis of spectral features showed that LIG532 spectral lines are narrower than that of the LIG355 sample (Table 2), indicating the presence of fewer structural defects in the LIG532 sample than in LIG355 one. This is followed by a significantly higher I(2D)/I(G) ratio (0.5, compared to 0.42 in LIG355), showing that, in this sample, the formed LIG structure is closer to a graphene-like crystal structure, as the high-intensity 2D band is a prominent feature of multilayer graphene structures.

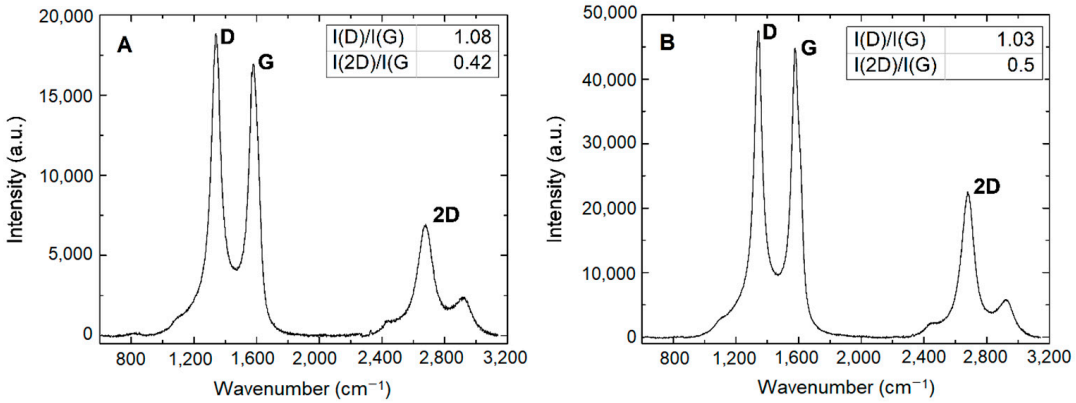

Figure 4. Measured Raman spectra of LIG355 (**A**) and LIG532 (**B**) samples.

Table 2. Spectral lines FWHM for LIG355 and LIG532 samples.

Sample	LIG355	LIG532
FWHM (D), cm^{-1}	88.2	79.7
FWHM (G), cm^{-1}	77.6	71.5
FWHM (2D), cm^{-1}	131	106.4

CV was initially used for the characterisation of the LIG electrodes using $K_4[Fe(CN)_6]$ as a redox probe in 0.1 M KCl/HCl pseudo-buffer solution, pH 2.0, at different potential scan rates. As seen in Figure 5A,B, the peak-to-peak separation changed from 160 to 414 mV and from 107 to 385 mV at LIG355 and LIG532, respectively, depending on the potential scan rate. As seen, it is not close to one electron Nernstian slope. The redox peak height ratio was between 0.68 and 0.87 at LIG355, and at LIG532 was around 1.12, which indicated a quasi-reversible redox reaction. The peak current density was linearly dependent on the square root of the potential scan rate meaning that the process is controlled by diffusion. The slopes of these linear dependencies were 2.07 and -1.90 mA cm^{-2} $V^{-1/2}$ $s^{1/2}$ at LIG355 and 2.24 and -2.66 mA cm^{-2} $V^{-1/2}$ $s^{1/2}$ at LIG532 for oxidation and reduction, respectively.

As was discussed by the electrochemical community about the charge transfer in thin films diffusion and diffusion-controlled electrochemical processes a decade ago, the peak-to-peak separation is not related to the electrocatalytic effect but to a semi-infinite diffusion [32,33]. If a double logarithmic plot of peak current versus the scan rate has a gradient of 0.5 or close to it, the electrochemical response is governed by the Randles–Ševčik equation and is purely diffusional [32]. Figure 5D depicts the double logarithmic plot of the linear dependence of oxidation peak current density on the scan rate (Figure 5C) at bare LIG electrodes. The slope of this dependence for LIG355 was 0.572, and for LIG532 was 0.546. The value was similar to that of an ideal semi-infinite diffusion [32,33]. According to these facts, the electrochemical processes at LIG355 and LIG532 depend on the semi-infinite diffusion; therefore, the Randles–Ševčik equation can be applied to the determination of A_{EA}, which was found to be 0.773 cm^2 and 0.879 cm^2 at LIG355 and LIG532, respectively. As seen, A_{EA} was larger than the geometric one (0.5 cm^2) for both samples due to the rough electrode surface (Figure 3A,B).

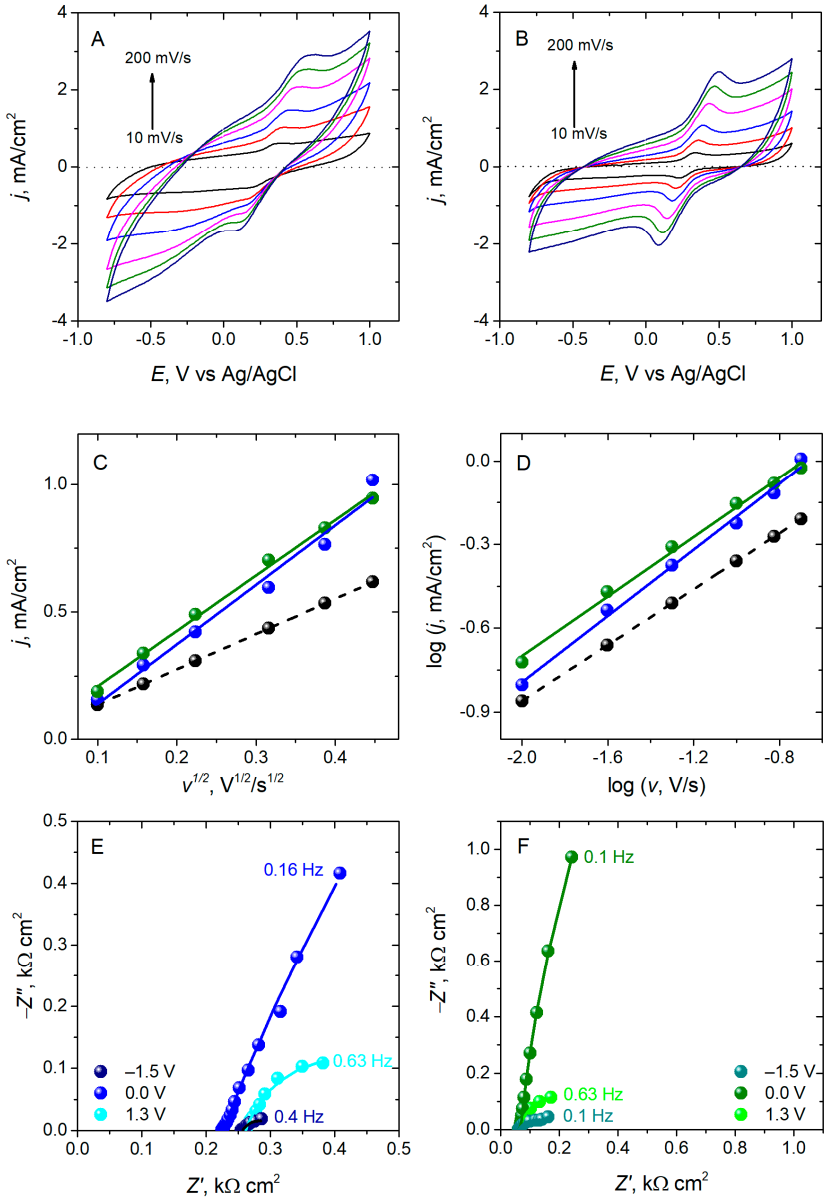

Figure 5. CVs at LIG355 (**A**) and at LIG532 (**B**) in 0.1 M KCl/HCl, pH 2.0, a solution with 2.0 mM $K_4[Fe(CN)_6]$ at different scan rates (10, 25, 50, 100, 150, and 200 mV s^{-1}). Dependencies of the current density of the oxidation peak on the square root of scan rate (**C**) and the logarithm of current density on a logarithm of scan rate (**D**) at LIG355 (dark blue) and LIG532 (dark green) electrodes. Dashed black line represents the predicted current based on the Randles–Ševčik equation and the geometric surface area of the bare electrode. Complex plane impedance spectra at LIG355 (**E**) and LIG532 (**F**) in 0.1 M PBS solution of pH 7.0, at different potentials: −1.5 V, 0.0 V, and +1.3 V.

EIS spectra were also registered at LIG electrodes to analyse electrochemical processes at the electrode–electrolyte interface. The potentials were set according to the CV (Figure 5E,F): most negative potential applied −1.50 V, most positive potential +1.30 V, and 0.0 V, which is in the double layer region. As expected, capacitive behaviour was observed in the double layer region (Figure 5E, blue symbols), while charge transfer observed by semicircles in spectra dominated at the potential of oxidation (+1.3 V, Figure 5E, light blue symbols) and reduction (−1.5 V, Figure 5E, dark blue symbols). Hydrogen evolution occurred by forming gas bubbles at −1.5 V, and, therefore, the spectrum at low frequencies was scattered, and the last points were omitted. No clear semicircle was found in the high-frequency region, which is often observed at carbon nanomaterial electrodes [34].

EIS spectra at LIG532 were also recorded at the same potentials, as depicted in Figure 5F. The spectra had the same tendency as in the case of LIG355. However, a clear charge occurred in the double layer region separation, indicated by a straight line at 0.0 V, Figure 5F, green symbols. Misshaped semicircles were obtained for oxidation and reduction, indicating charge transfer. Moreover, the spectrum was uniform (Figure 5F, dark green symbols) at the reduction and hydrogen evolution potential, and gas bubbles did not interfere in this case, indicating a different surface structure than at the above-discussed electrode. Furthermore, small misshaped semicircles are visible in the spectra in the high-frequency regions, meaning that carbon nanostructured materials are formed at LIG532. This fact also confirms Raman spectroscopy data that LIG532 has graphene-like structures.

The spectra were analysed by fitting to equivalent electrical element circuits, as shown in Figure S1. The fitting errors were less than 5%. For LIG355, a "simple" circuit (Figure S1A) consisting of the cell resistance, R_Ω in series with the parallel couple of the charge transfer resistance, R_{ct}, and CPE as non-ideal capacitance (Equation (1)).

$$CPE = \frac{-1}{(Ci\omega)^\alpha} \quad (1)$$

where C is an ideal capacitor, ω—is the angle in radians, and α the roughness is the exponent due to the heterogeneity of the surface [35]. The exponent $\alpha = 1$ means an ideal capacitor and perfectly flat surface. C acted in this case as a double-layer capacitor, C_{dl}.

The R_Ω was ca. 250 Ω cm^2 and did not depend on the applied potential. As expected, the highest R_{ct} was in the double layer region (at 0.00 V)—6.74 kΩ cm^2 and the lowest +1.3 V—0.310 kΩ cm^2, while at −1.50 V it was 0.055 kΩ cm^2, showing that the most difficult charge transfer was where oxygen generation took place. The roughness factor was ca. 0.878 and did not depend on the applied potential, showing that the interface was rather rough. Capacitance recalculated from CPE using Equation (1) had an opposite tendency to R_{ct}, and it was the lowest in the double layer region—0.471 mF cm^{-2}, followed by 1.22 mF cm^{-2} at +1.3 V and 2.93 mF cm^{-2} at −1.5 V.

The same equivalent circuit was not fitting to the spectra at LIG532. These spectra were analysed with the Randles equivalent circuit, which is extended with an open Warburg element (W_o, Equation (2)) as shown in Figure S1B. It shows that diffusion of the electroactive species played an important role at these electrodes.

$$W_o = \frac{R_{dif} cot\left([i\tau\omega]^\alpha\right)}{(i\tau\omega)^\alpha} \quad (2)$$

where R_{dif} is the diffusion resistance, τ is the time constant depending on the diffusion rate ($\tau = l^2/D$, where l is the effective diffusion thickness, and D is the effective diffusion coefficient of the species), and $\alpha = 0.5$ for a perfect uniform flat interface. At high frequencies, the impedance behaviour is that of infinite diffusion (phase angle 45°), and at low ones, it tends to be that of a capacitor (phase angle 90°). Values of α of less than 0.5 express the fact that the interface is not uniform [35].

At LIG532, R_Ω was ca. 60 Ω cm^2 and did not depend on the applied potential. R_{ct} had the same tendency as in the case of LIG355: 12.2 (0.00 V) > 0.255 (+1.30 V) > 0.100 kΩ cm^2 (−1.50 V). The interface was rather flat at this electrode because the exponent α was close to 1 (from 0.980 to 0.999). The CPE changes were similar to those at LIG355; however, after recalculation to capacitance, the tendency was reformed: 1.17 (+1.30 V) < 1.27 (0.00 V) < 9.44 mF cm^{-2} (−1.50 V).

Parameters calculated from W_o are given in Table S1. R_{dif} has changed depending on the applied potential also in the opposite sequence as R_{ct}: 21.5 (0.00 V) < 77.6 (+1.30 V) < 707 Ω cm^2 (−1.50 V), the electrode was rather porous according to the exponent α obtained from W_o, which was ca. 0.44. The diffusion time was in the millisecond range. The porous nature of LIG532 is visible from the spectra, as also discussed by Lasia in [36]. The author identified and modelled the pore shape by analysing EIS spectra but did not use the

Warburg element. Since diffusion is an important factor at porous surfaces, the majority of models implement Warburg elements in their models [37]. W_o was used by Nguyen and Breitkopf to analyse the spectra of microporous materials [38]. They could determine the gas diffusion coefficient to a porous material from a modified Warburg model.

In summary, LIG355 had a rough surface while LIG532 had a microporous surface, as was observed from Raman spectroscopy and SEM showing graphene-like structures.

3.2. Optimisation of Electrode Modification with Polyfolate

The previous study [23] showed that PFA is suitable for pH detection in the range between 6 and 9. LIG electrodes are flexible and composed of graphitic materials suitable for electrochemical applications, such as sound in 3.1. These electrodes could probably also be used for pH detection where glass electrodes are not convenient.

Electropolymerisation was performed at bare LIG electrodes using a previously optimised protocol [23], as described in Section 2.3.

The number of CV cycles and the potential range were adjusted for these electrodes. As observed previously [23], Chit improves PFA stability significantly; therefore, LIG electrodes were also drop-coated with a Chit layer, which improves PFA adhesion to the electrode surface. The polymerisation CVs are presented in Figure 6. As expected, growth of the current density with the number of CV cycles was detected at all electrodes. Only small peaks were registered in the first few cycles, but after a few cycles, peaks were visible, and the current density increase at Chit/LIG was faster than that at bare LIG. The influence of the Chit layer on the current density growth at final potential (+1.5 V) was different for both LIG electrodes: it was lower at Chit/LIG355 than at bare LIG355, but it was higher at Chit/LIG532 than at LIG532. These differences are attributed to the morphological and structural changes of LIG electrodes. The polymerisation was performed until the current density ranged to a steady state (Figure S2). It was found that 75 cycles were optimal at LIG355 and 72 cycles at LIG532.

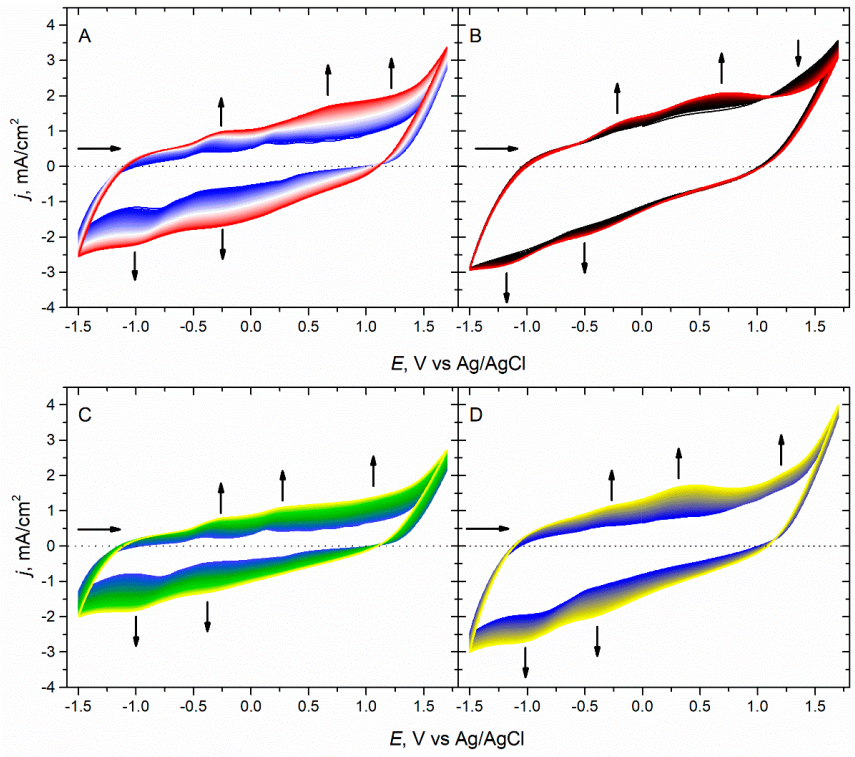

Figure 6. CVs of electropolymerisation of 1.0 mM FA at LIG355 (**A**), Chit/LIG355 (**B**), LIG532 (**C**), and Chit/LIG532 (**D**), respectively, in 0.1 M PBS, pH 6.0. The potential interval between −1.5 V and +1.7 V, number of cycles 75 (**A**,**B**) and 72 (**C**,**D**). Vertical arrows show changes in current with the number of cycles, and horizontal arrows indicate the direction of the potential scan.

3.3. Characterisation of Modified LIG Electrodes

PFA-modified LIG electrodes were first characterised by employing microscopies and wettability studies. Optical microscopy of bare LIG355 (Figure 7A) shows a rough surface with obscure laser left lines. As seen from Figure 7B, Chit coating on LIG355 is more expressed along laser-produced lines making them more visible. After FA electropolymerisation on the Chit/LIG355 surface (Figure 7C), the topography is different from that of bare LIG, and the Chit film is less visible. Moreover, it seems that the gaps between Chit are filled with PFA; however, most probably, the Chit structure is changed during the electropolymerisation of FA. A different picture was observed on bare LIG532 (Figure 7D), where the surface shows crack-like structures. The coating with Chit (Figure 7E) fills pits and irregularities and forms a net-like structure. After FA electropolymerisation on Chit/LIG532 (Figure 7F), Chit films are no longer seen, but thick-looking polymer fibre-like structures are observed.

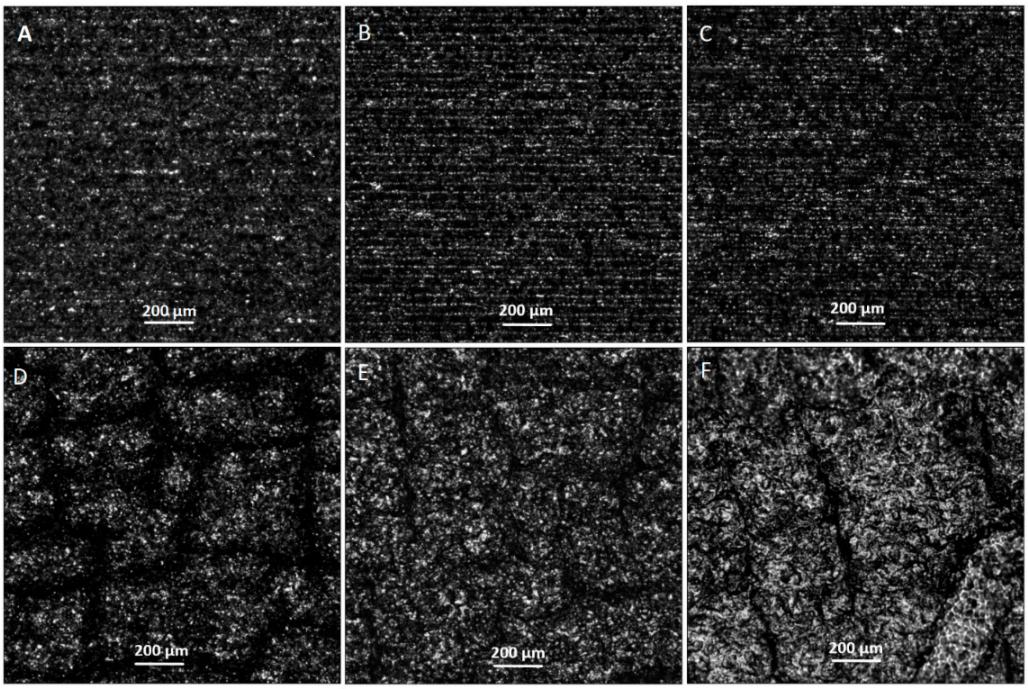

Figure 7. Optical microscopy images of bare LIG355 (**A**) and LIG532 (**D**), Chit/LIG355 (**B**) and Chit/LIG532 (**E**), and PFA/Chit/LIG355 (**C**) with PFA/Chit/LIG532 (**F**). Magnification is 10× in all cases.

SEM images are similar to those of optical microscopy of the same electrodes. LIG structure lines are seen clearly in the image (Figure 8A) of the bare LIG355 surface. Meanwhile, the bare LIG532 (Figure 8D) possesses a disordered graphene-like structure, and no laser lines are visible. Further, after coating LIG355 with Chit (Figure 8B), graphene structures are covered with net-like film. When the LIG532 surface is coated with Chit film (Figure 8E), it creates a uniform surface with no graphene structures visible. PFA/Chit/LIG355 exhibits an ordered surface with fibre-like polymer structures (Figure 8C). The addition of PFA on top of Chit/LIG532 made the film rigid, which was de-attached in a vacuum chamber of SEM and was torn apart; therefore, it was not possible to investigate the surface topography of this modification.

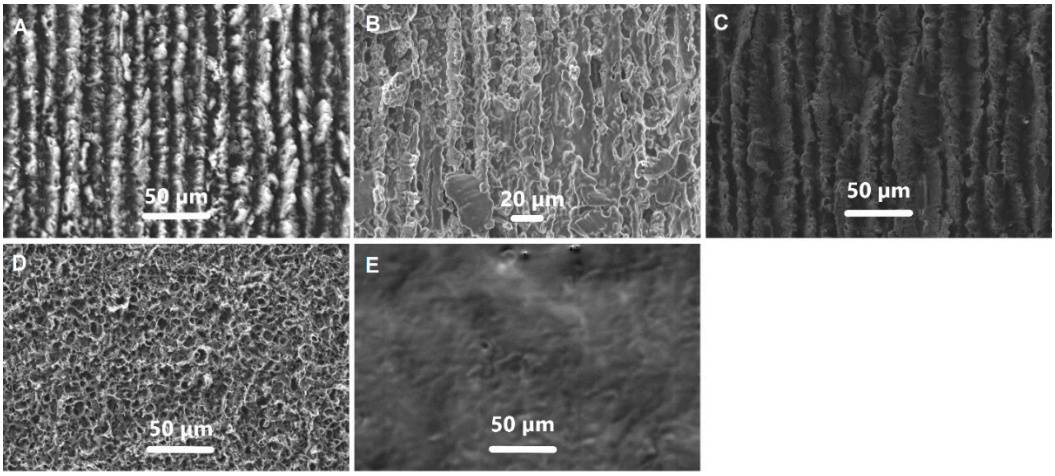

Figure 8. SEM 500× (**A**,**C**–**E**) and 600× (**B**) images of modified LIG electrodes surface (**A**–**E**) of bare LIG355 (**A**) and LIG532 (**D**), Chit/LIG355 (**B**) and Chit/LIG532 (**E**), and PFA/Chit/LIG355 (**C**).

Hydrophilicity was studied by measuring the water drop contact angle measured over 6 s using 1 and 3 µL of Milli-Q water. The contact angle was registered under dynamic conditions within 6 s (Figure 9) [39]. As is well known, if the contact angle is <90° surface is hydrophilic, and when it is >90° surface is hydrophobic [40]. Firstly, the contact angle measured immediately after the drop was set on LIG355 was 83.28 ± 3.93°, but within 6 s, it dropped to 31.21 ± 1.56°. The situation was different on LIG532, where the contact angle changed from 57.85 ± 15.85° (0 s) to 41.72 ± 8.93° (6 s). These facts lead to the conclusion that the unmodified LIG surface is hydrophilic due to the structural properties of the surface. Most probably, the hydrophobicity is due to a high porosity of LIG which was observed using SEM (Figure 3) and EIS (see below). Application of the Chit layer on LIG electrodes made the surface hydrophobic; the contact angle on Chit/LIG355 changed from 120.03 ± 0.87° to 115.44 ± 2.26°, and on Chit/LIG532 from 111.42 ± 4.73° to 107.99 ± 3.59°. Although hydrophilic properties would be expected for Chit films, this is not the first case when hydrophobic Chit film was obtained, and this phenomenon is explained by the reorientation of functional groups during drying and hydrogen bond formation, which is more thermodynamically favourable [41].

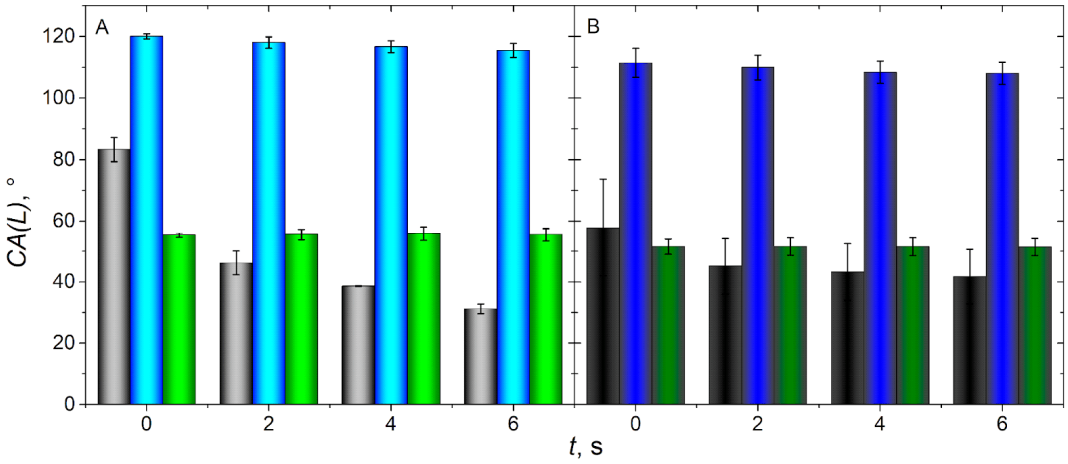

Figure 9. Contact angle changes with time (up to 6 s) on differently modified LIG355 (**A**) and LIG532 (**B**) electrodes: bare LIG (grey bars at LIG355 or black bars at LIG532); Chit/LIG (light blue bars at LIG355 or dark blue bars at LIG532), and PFA/Chit/LIG (light green bars at LIG355 or dark green bars at LIG532). Measurement method: sessile drop; drop phase: water; surrounding phase: air; used volume: ~1.0 µL on bare electrodes and ~3.0 µL on modified ones.

As expected, further modification with PFA again caused the hydrophilic nature of the electrode: the contact angle was between 55.28 ± 0.75° and 55.45 ± 2.11° (within 6 s) on PFA/Chit/LIG355 and between 51.48 ± 2.49° and 51.39 ± 2.81° on PFA/Chit/LIG532.

CVs of LIG electrodes modified with Chit film showed no significant changes compared with the bare LIG electrodes. At LIG355, the current density was slightly larger than that without Chit (Figure 5), and at LIG532, the increase was significantly larger (Figure 10A,B) because Chit is an electroactive polymer. Due to the diffusion barrier caused by the polymer, the peak separation increased compared to that without Chit, and depending on the potential scan rate, it changed between 228 and 900 mV and between 177 and 859 mV at Chit/LIG355 and Chit/LIG532, respectively, while the ratio of the redox peak heights was close to 1.0. Again, the peak current density had a linear dependence on the square root of the potential scan rate, and the slopes were 2.56 and −2.07 mA cm^{-2} $V^{-1/2}$ $s^{1/2}$, and 7.13 and −7.34 mA cm^{-2} $V^{-1/2}$ $s^{1/2}$ at Chit/LIG355 and Chit/LIG532, respectively.

Even after electrode modification, the CV behaviour showed the semi-infinite diffusion found from the double logarithmic plot of linear dependence of oxidation peak current density from the scan rate (Figure 10E,F) as at Chit/LIG electrodes. The slope of this dependence for Chit/LIG355 was 0.590, and for Chit/LIG532 was 0.602. Although the value was slightly higher than that of the bare electrodes, they are still close to the theoretical value, and the Randles–Ševčik equation can be used to determine A_{EA}, which was 0.933 cm^2 at Chit/LIG355 and 2.732 cm^2 at Chit/LIG532, i.e., significantly larger than at bare electrodes.

Figure 10C,D depicts the electrochemical behaviour at PFA/Chit/LIG355 and PFA/ Chit/LIG532, respectively, at different scan rates under the same conditions as in the case of the previous electrodes. Although PFA is a redox compound, no clear redox peaks were observed in CV, as observed in the previous work [19]; therefore, the additional redox probe was used. Since CVs profiles were misshaped at the potential scan rates faster than 50 mV s^{-1}, the modified electrodes were studied in the scan rate range from 5 to 50 mV s^{-1}. The CV profile was similar to the electrode modified with Chit, but the current density at PFA/Chit/LIG355 (Figure 10C) was almost twice higher than that without PFA. In the case of PFA/Chit/LIG532, the current density was pretty much the same as without PFA; the only difference was that the peak-to-peak separation PFA-modified electrode was larger for the same scan rates (Figure 10D). The peak-to-peak separation varied from 275 to 932 mV and from 290 to 921 mV at PFA/Chit/LIG355 and PFA/Chit/LIG532, respectively, depending on the potential scan rate. The electrochemical behaviour of these electrodes mostly depends on the nature of the substrate. Moreover, PFA acts more as a semiconducting polymer [19].

As seen, the linear dependence of the current density is on the square root of the potential scan rate with the slopes of 10.51 and −10.78 mA cm^{-2} V s^{-1} (Figure 10C) and 9.06 and −9.23 mA cm^{-2} $V^{-1/2}$ $s^{1/2}$ (Figure 10D), for oxidation and reduction, respectively, indicating that the process is dominated by diffusion, differently from those observed in the previous works [19,21]. The ratio of the redox peak current densities was close to 1.0. The double logarithmic plot of linear dependence of oxidative peak current density from the scan rate (Figure 10E,F) had slightly lower slopes than for Chit/LIG electrodes: 0.466 and 0.479 for PFA/Chit355 and PFA/Chit532, respectively, again indicating semi-infinite diffusion. A_{EA} were 3.808 and 3.282 cm^2 at PFA/Chit/LIG355 and PFA/ChitLIG532. These facts show that each polymer layer increases the electroactive area.

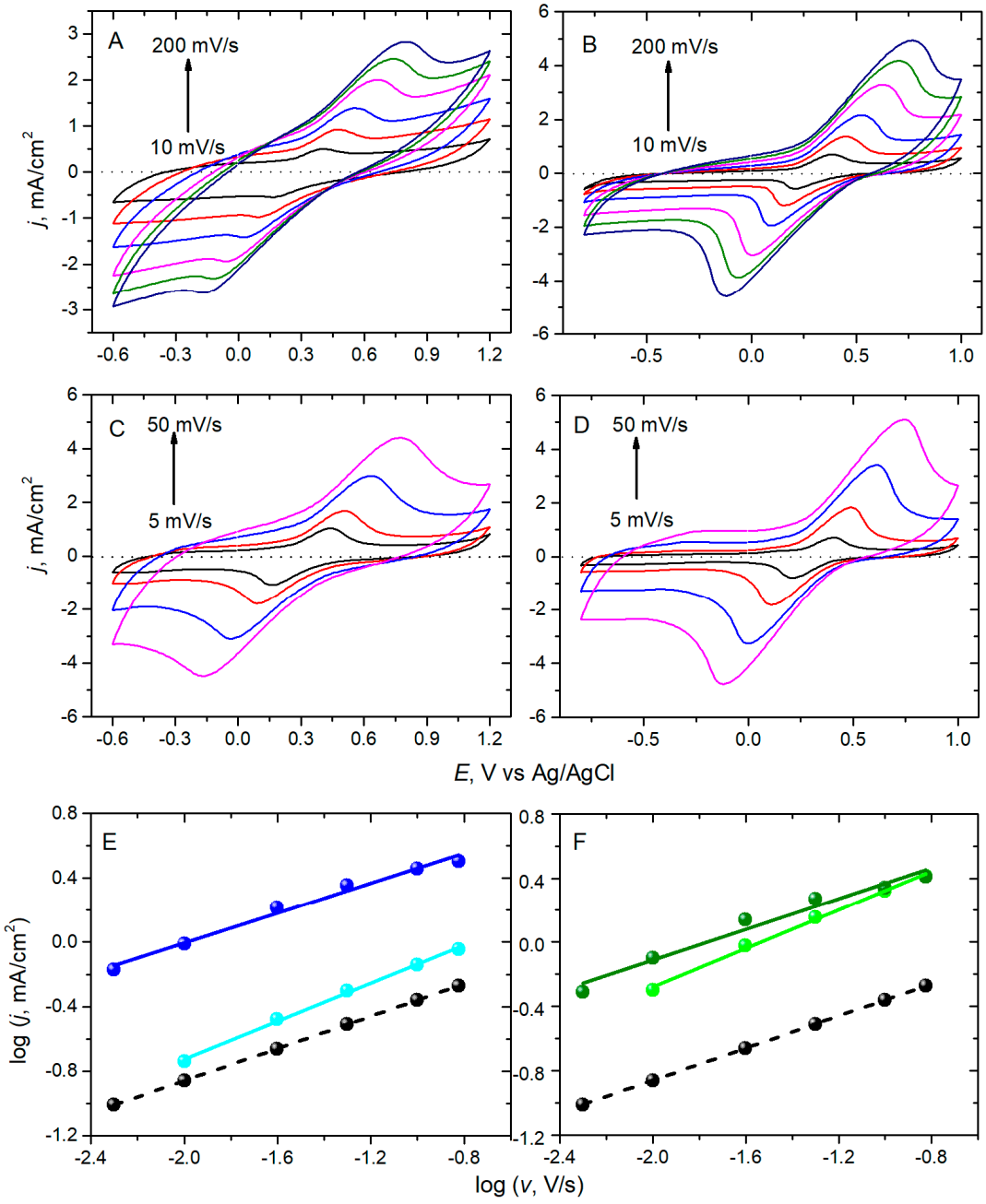

Figure 10. CVs at Chit/LIG355 (**A**), PFA/Chit/LIG355 (**C**), Chit/LIG532 (**B**), and PFA/Chit/LIG532 (**D**) in 0.1 M KCl/HCl, pH 2.0 solution with 2.0 mM $K_4[Fe(CN)_6]$ at different scan rates: 10, 25, 50, 100, 150, and 200 mV s^{-1} (**A**,**B**) and 5, 10, 25, and 50 mV s^{-1} (**C**,**D**). Double logarithmic plot of oxidation peak versus scan rate at modified LIG355 ((**E**), light blue coated with Chit and dark blue with PFA/Chit) and LIG532 ((**F**), light green coated with Chit and dark green with PFA/Chit), respectively. The black line represents the predicted current based on the Randles–Ševčik equation and the geometric surface area of the bare electrode.

EIS spectra were recorded to analyse interface processes at each sensor preparation step at different potentials. The potentials were chosen according to the data obtained from CV: the polymer reduction and oxidation potentials: −0.74 and +0.43 V, respectively, and in the double layer region at 0.0 V. Since EIS spectra at modified LIG355 were too scattered, this method was used only for modified LIG532 electrodes. The spectra are depicted in

Figure 11. Since spectra had small semicircles in a high-frequency region which is not visible in this scale, it was depicted in Figure S3.

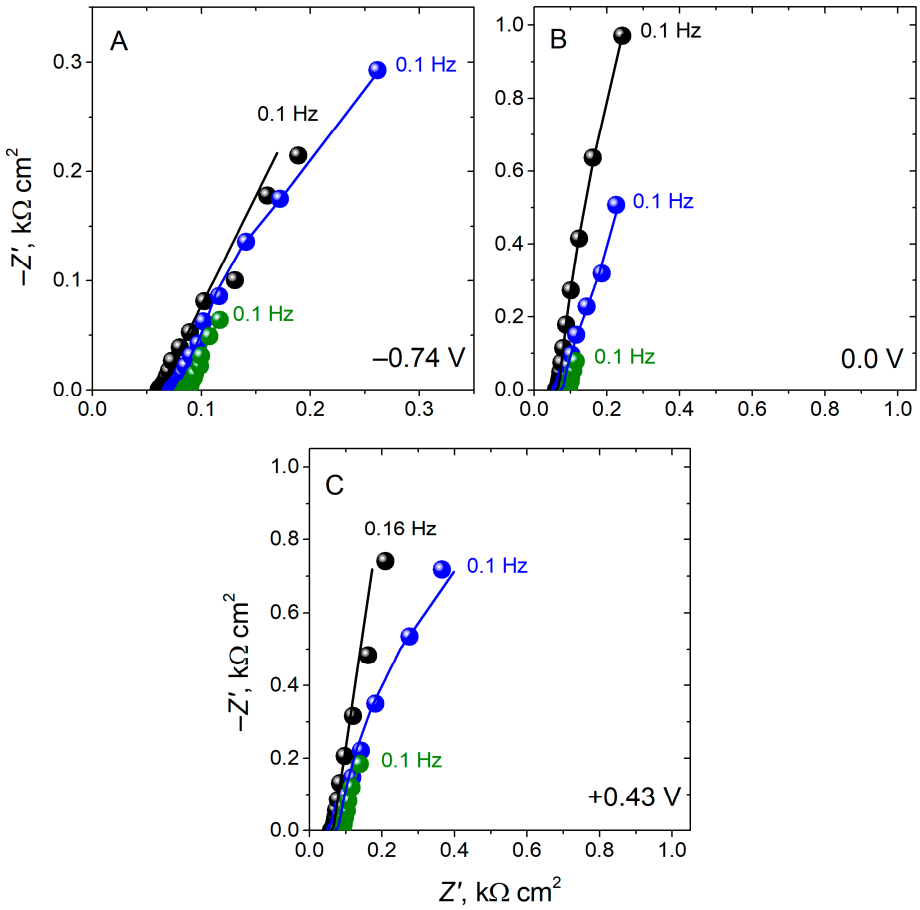

Figure 11. Complex plane spectra at LIG532 (black symbols), Chit/LIG532 (blue symbols), and PFA/Chit/LIG532 (green symbols) in 0.1 M PBS solution of pH 7.0 at different potentials: −0.74 V (**A**), 0.0 V (**B**), and +0.43 V (**C**).

EIS spectra of modified LIG532 were analysed using various equivalent circuits, depending on potential and electrode modification, and they are given in Figure S1B,C. The parameters calculated from equivalent circuits are summarised in Table S2.

The Chit/LIG532 spectra were analysed by fitting to Randles equivalent circuit. Although Chit would be expected to cover electrode pores, this film acts as a diffusion barrier by itself. R_Ω increased in ca. 10 Ω cm^2 at each modification step from the bare electrode to PFA/Chit/LIG532. R_{ct} was the biggest at Chit/LIG532 at all potentials due to the electrochemical properties of Chit film, which is electroactive but has lower electroconductivity. The lowest R_{ct} was observed at the bare electrode, and after the modification with PFA, it again decreased (Table S2). A similar tendency was observed for C_{dl}, except in the double-layer region, where capacitance was lowest at Chit/Lig532, where only charge separation took place.

At PFA/Chit/LIG532, the influence of diffusion was low because the spectra did not fit Randles equivalent circuit, except for the reduction peak position (−0.74 V). In other cases, the R-C parallel couples were extended with film CPE in series, as depicted in Figure S1C. This apparently happened due to conducting PFA film, which restructured Chit film, as also visible from morphology changes, Figures 7F and 8C. Most probably, PFA also enters or mixes together with Chit and reduces the diffusional barrier. However, it depends on applied potential: diffusion of electroactive species was still playing an important role

at PFA/Chit/LIG532 −0.74 V. Film capacitance from CPE at the low-frequency region was not analysed for PFA/Chit/LIG532.

The analysis of diffusion parameters from Warburg element showed that at −0.74 V, R_{dif} was similar at both Chit/LIG532 and PFA/Chit/LIG532, and the diffusion time constant was more than 1 s (Table S2), indicating a different film structure than that at other potentials studied. Diffusion of electroactive species was significantly faster at Chit/LIG532 at 0.00 V, which was ca. 60 ms, while it was ca. 130 ms at +0.43 V. Meanwhile, R_{dif} was also related to faster diffusion, and it was much lower than that at −0.74 V, and it reached ca. 28 Ω cm^2. The film was rather heterogeneous because the homogeneity coefficient was less than 0.5. Such a coefficient value is rather usual for film electrodes [35].

3.4. Response to pH

3.4.1. Sensor Performance

pH measurements were performed employing potentiometry, which is a precise and common method for electrochemical pH determination [23]. A conventional potentiometric approach was used to determine pH in the interval from 6.0 to 9.0. The response is demonstrated in Figure 12. As seen, the forward and backward response is the same, with the exception of the first test. This means that the electrode needs preconditioning before the application in practice. Other measurements are reproducible, and the reproducibility for both PFA/Chit/LIG355 and PFA/Chit/LIG532 is 96.5 ± 0.1%. The sensitivity, or in other words, the Nernstian slope, for PFA/Chit/LIG355 is 26.89 ± 0.97 and 28.83 ± 0.65 mV/pH in the forward and backward determination, respectively, while the mean value is 27.86 ± 0.81 mV/pH. The sensitivity is 30.32 ± 0.50 mV/pH in both directions for PFA/Chit/LIG532, in comparison with the sensitivity of PFA and Chit-modified pyrolytic graphite electrode which was discussed in the previous work [23], was 43.5 ± 2.6 mV/pH. As seen, the sensitivity was higher than that of LIG electrodes, but it was neither flat nor flexible. The slope is not close enough to the e: H^+ Nernstian one; nevertheless, PFA/Chit/LIG532 is suitable for use in practical applications, e.g., for physiological fluids such as blood or urine.

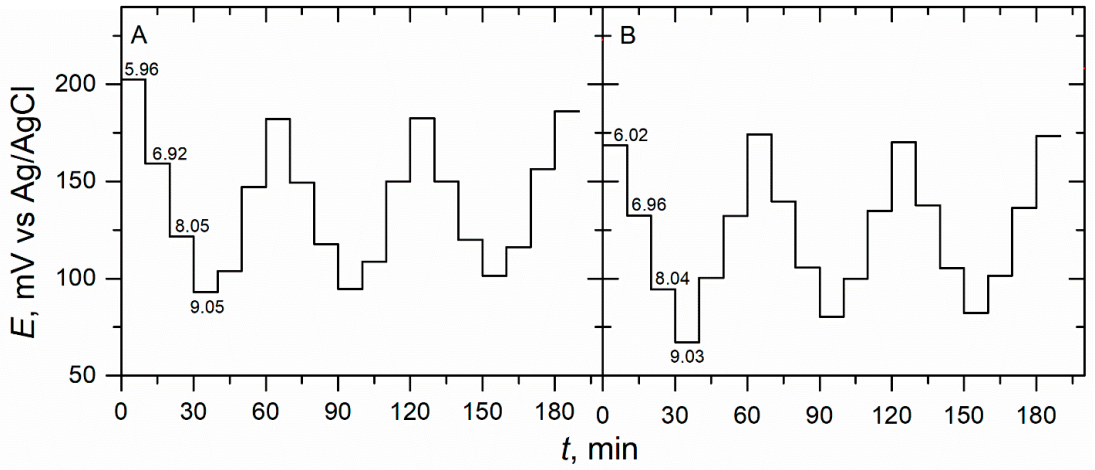

Figure 12. PFA/Chit/LIG355 (**A**) and PFA/Chit/LIG532 (**B**) potential dependence on pH in 0.1 M PBS solutions from pH 6.0 to 9.0.

Compared to other LIG electrodes for pH detection, the LIG532 and especially the LIG355 have significantly lower sensitivity. For example, the potentiometric pH sensor developed by Rahimi et al. [42] using carbonised PI and modified with polyaniline displays a much better linear sensitivity of 53 mV/pH with stable performance in the physiological range of pH 4–10. Even better sensitivity to pH (66 mV/pH) was observed using LIG modified with Au nanoparticles in the pH range from 4 to 7.4 as a voltammetric sensor [43]. A similar LIG-based sensor employing riboflavin in solution for voltammetric pH detection

had a sub-Nernstian slope of 56 mV/pH in the pH range from 3 to 8 [16]. Nevertheless, recently published work by Lampinen et al. [44] on LIG application for pH detection as a field effect transition sensor reported a lower slope of 25 mV/pH in the pH range of 6.8–9.5.

3.4.2. Stability, Reproducibility, and Selectivity of pH Sensor

The stability of LIG electrodes modified with PFA was investigated by employing potentiometry in 0.1 M PBS solutions from pH 6.0 to 9.0. Each measurement was repeated 3 times in sequence with a few day intervals starting from ca. one week after electrode preparation—the first week was used for other electrode characteristics.

PFA/LIG electrodes were mechanically destroyed after ca. 20 days; therefore, no more measurements were possible. The sensitivity at PFA/LIG355 was 28.41 ± 1.01 mV/pH, and it remained the same until the electrode was destroyed (after 2 weeks). In the case of PFA/LIG532, the sensitivity was 34.27 ± 2.09 mV/pH, but it slightly dropped down (to 30.24 ± 1.99 mV/pH) after two weeks. To increase the stability, the LIG surface was coated with Chit prior to FA polymerisation, expecting that the surface would have more functional groups of PFA to adhere to. This improvement resulted in increased stability at both PFA/Chit/LIG355 and PFA/Chit/LIG532, and the signal was stable for at least 50 days. The sensitivity decreased from 27.86 ± 0.97 to 21.86 ± 0.43 mV/pH for PFA/Chit/LIG355 in 50 days. Such a decrease was smaller at PFA/Chit/LIG532, and the sensitivity dropped from 30.32 ± 0.06 to 28.14 ± 0.25 mV/pH after 50 days.

Although the sensitivity at the electrodes without Chit was significantly higher, especially in the case of LIG532 (Table 3), the stability was significantly better when LIG was modified with Chit (Figure 13). Moreover, as seen in Table 3, the use of Chit slightly decreased the sensitivity of modified electrodes and increased the repeatability of the signal (observed from deviation of the sensitivity values), especially in the case of LIG532.

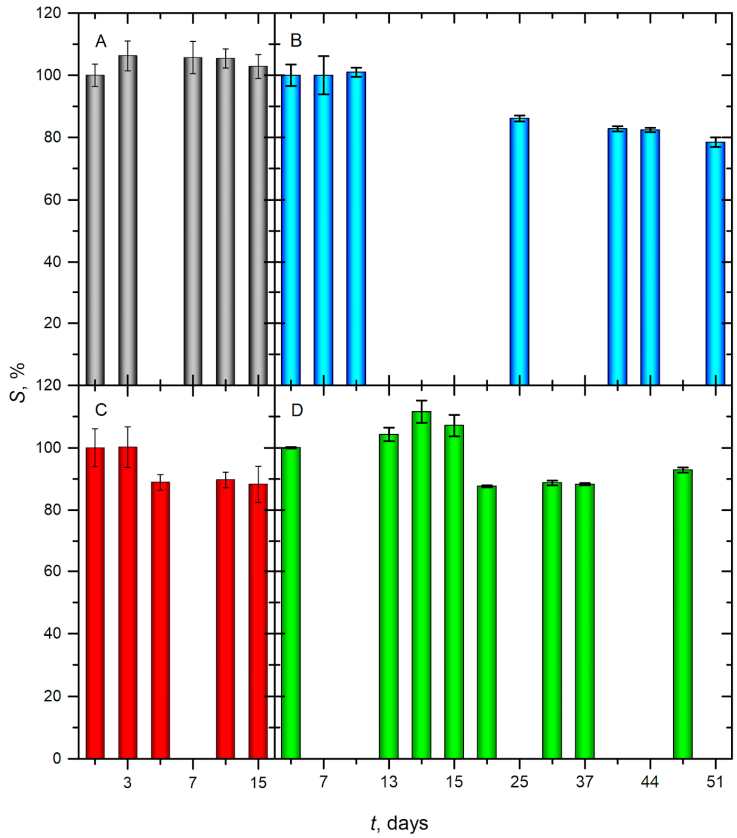

Figure 13. Stability of modified LIG electrodes calculated from the sensitivity (S). PFA/LIG355 (**A**), PFA/LIG532 (**C**), PFA/Chit/LIG355 (**B**), and PFA/Chit/LIG532 (**D**). Response to pH obtained from potentiometry in 0.1 M PBS solutions from pH 6.0 to 9.0 after 600 s.

Table 3. Sensitivity of modified LIG electrodes on the first day of measurements.

Electrode	Sensitivity, mV/pH
PFA/LIG355	28.41 ± 1.01
PFA/LIG532	34.27 ± 2.09
PFA/Chit/LIG355	27.86 ± 0.97
PFA/Chit/LIG532	30.32 ± 0.06

The reproducibility of 3 electrodes was ca. 30% for PFA/Chit/LIG355 and 3.25% for PFA/Chit/LIG532, indicating that the 355 nm laser was not suitable for the production of reliable LIG electrodes.

The selectivity of PFA/Chit/LIG355 and PFA/Chit/LIG532 was tested using interferents usually present in the food industry. Single valent ions such as Na^+, $K^{+,}$ and NH_4^+ and organic compounds such as citric acid and glucose were used as interferents. As seen in Figure 14, interference of K^+ was +5.96% at PFA/Chit/LIG355, but at PFA/Chit/LIG532, it was −1.39%. Furthermore, the interference from other used ions and organic compounds was 10.1 ± 0.72%, and 2.63 ± 0.50% at PFA/Chit/LIG355 and PFA/Chit/LIG532, respectively. As seen, the interferants at PFA/Chit/LIG532 had a lower impact than that at PFA/Chit/LIG355.

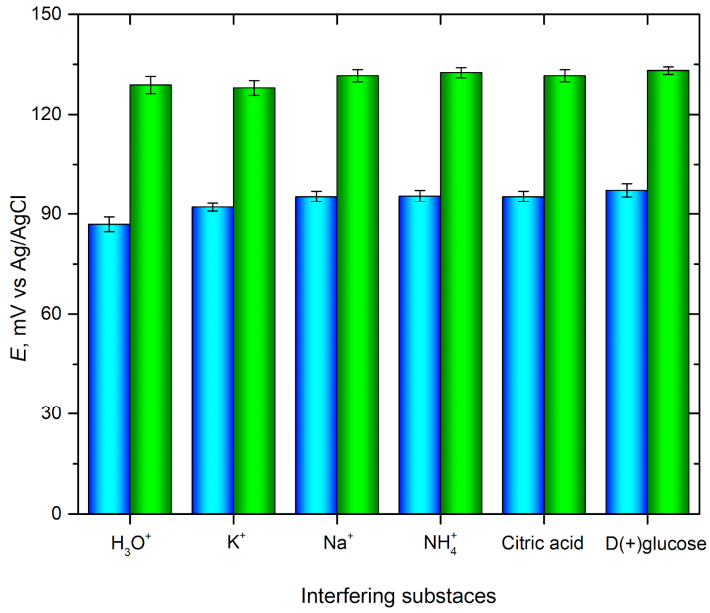

Figure 14. Interference studies of 1.0 mM of single valent ions K^+, Na^+, NH_4^+, and some organic compounds 0.1 mM citric acid and D(+)glucose, at PFA/Chit/LIG355 (blue bars) and PFA/Chit/LIG532 (green bars), to the potentiometric response to protons. Supporting electrolyte 0.1 M PBS, pH 7.0, accumulation time 600 s.

3.4.2.1. pH Determination in Real Samples

Finally, a 0.1 M PBS was prepared by randomly mixing buffer precursors to obtain a solution of unknown pH; also, the pH of 1 M Tris hydrochloride and 0.1 KCl solutions was determined. Afterwards, the pH of this solution was measured with PFA/Chit/LIG355 and PFA/Chit/LIG532. Obtained results were compared with the conventional pH meter with a glass electrode. The results are presented in Figure S4. The deviations from the values obtained with the pH meter were from −0.02 to −0.08 for PFA/Chit/LIG355 and +0.04 for PFA/Chit/LIG532 (in all cases n = 3). As seen, both electrodes were reliable in the pH range studied.

4. Conclusions and Perspectives

LIG modified with PFA, which was stabilised with Chit film underneath, was used as a base to develop a flat and flexible pH sensor. Electrode characterisation and testing led to the following conclusions.

1. Microscopic imaging revealed that bare LIG electrodes had rough structures after laser treatment giving hydrophilic properties, and PFA forms fibre-like structures on Chit coated LIG.
2. Electrochemical investigation with the redox probe demonstrated that diffusion is a limiting process at the bare and modified LIG electrodes. A capacitive behaviour was observed from EIS spectra at bare electrodes showing a rather rough interface at LIG355 but a microporous one at LIG532 in the negative and positive potential regions. Diffusion of electroactive species was observed at Chit/LIG532 because the Randles equivalent circuit was fitting the spectra. However, this equivalent circuit was not fitting to the PFA/Chit/LIG532 spectra because diffusion was not a limiting step at this modified electrode.
3. The developed flat and flexible electrode was sensitive to pH in the region from 6.0 to 9.0. In the studied pH range, the sensitivity was 27.86 $\pm$ 0.81 for PFA/Chit/LIG355 and 30.32 $\pm$ 0.50 mV/pH for PFA/Chit/LIG532 with moderate stability for a period of more than two months.
4. The deviation from pH-meter values was down to 1% for PFA/Chit/LIG355 sensor and down to 0.5% for PFA/Chit/LIG532 sensor. The disadvantage of PFA/Chit/LIG355 was just pure reproducibility in terms of voltammetric characterisation.

Supplementary Materials: The following supporting information can be downloaded at: https://www.mdpi.com/article/10.3390/chemosensors11060329/s1, Figure S1: Equivalent circuits used to analyse EIS spectra: A—"simple" circuit for analysis at LIG355, B—Randles circuit for LIG532, C—circuit for some modified LIG532 electrodes; Figure S2: Last 5 cycles of FA electropolymerisation presented in Figure 6 at LIG355 (A), Chit/LIG355 (B), LIG532 (C), and Chit/LIG532 (D) indicating steady-state current. Insets show a zoom of oxidation current. All other conditions are as in Figure 6. Figure S3: Complex plane spectra in the region of high frequencies at LIG532 (black symbols), Chit/LIG532 (blue symbols), and PFA/Chit/LIG532 (green symbols) in 0.1 M PBS solution of pH 7.0 at different potentials: −0.74 V (A), 0.0 V (B), and +0.43 V (C); Table S1: Warbug element parameters calculated at LIG532 from Figure 5F using an equivalent circuit depicted in Figure S1B; Table S2: Analysis of EIS spectra at modified LIG532 from Figure 11 using an equivalent circuit depicted in Figure S1C; Figure S4: Validation of PFA/Chit/LIG355 (blue colour) and PFA/Chit/LIG532 (green colour) sensors in solutions with different pH using calibration curves (n = 3). Empty circles show detected pH in test solutions with the respective sensors, and the dashed lines show values obtained with pH-meter: 6.83 pink (0.1 M KCl), 7.48 red (0.1 M PBS), and 8.35 orange (1 M Tris hydrochloride).

Author Contributions: Conceptualisation, V.Ž., R.T., K.R. and R.P.; methodology V.Ž., R.T., A.S. (Aivaras Sartanavičius), K.R., A.S. (Algirdas Selskis) and R.P.; software, V.Ž., R.T., K.R., A.S. (Aivaras Sartanavičius) and A.S. (Algirdas Selskis); validation, R.T., K.R., A.S. (Algirdas Selskis) and R.P.; formal analysis, R.P.; investigation, V.Ž., R.T., K.R., A.S. (Aivaras Sartanavičius) and A.S. (Algirdas Selskis); resources, R.P.; data curation, V.Ž. and R.P.; writing—original draft preparation, V.Ž., R.T. and R.P.; writing—review and editing, V.Ž., R.T., K.R., A.S. (Aivaras Sartanavičius), A.S. (Algirdas Selskis) and R.P.; visualisation, V.Ž. and R.T.; supervision, R.P.; project administration, R.P.; funding acquisition, R.P. All authors have read and agreed to the published version of the manuscript.

Funding: This research was funded by Lithuanian Research Council under the project BEGAMA via Grant No 01.2.2-LMT-K-718-03-0038.

Institutional Review Board Statement: Not applicable.

Informed Consent Statement: Not applicable.

Acknowledgments: Authors are grateful to Ieva Matulaitienė, for the access to Raman spectroscopy at the Laboratory of Spectroelectrochemistry of the Department of Organic Chemistry (FTMC, Lithuania). Also, the authors thank Tomas Rakickas for wettability measurements using contact angle characterisation.

Conflicts of Interest: The authors declare no conflict of interest.

References

1. Dixit, N.; Singh, S.P. Laser-induced graphene (LIG) as a smart and sustainable material to restrain pandemics and endemics: A perspective. *ACS Omega* **2022**, *7*, 5112–5130. [CrossRef] [PubMed]
2. Marengo, M.; Marinaro, G.; Kosel, J. Flexible temperature and flow sensor from laser-induced graphene. In Proceedings of the 2017 IEEE Sensors, Glasgow, UK, 27 October–1 November 2017; pp. 1–3. [CrossRef]
3. Rahimi, R.; Ochoa, M.; Yu, W.; Ziaie, B. Highly stretchable and sensitive unidirectional strain sensor via laser carbonization. *ACS Appl. Mater. Interfaces* **2015**, *7*, 4463–4470. [CrossRef] [PubMed]
4. In, J.B.; Hsia, B.; Yoo, J.H.; Hyun, S.; Carraro, C.; Maboudian, R.; Grigoropoulos, C.P. Facile fabrication of flexible all solid-state micro-supercapacitor by direct laser writing of porous carbon in polyimide. *Carbon* **2015**, *83*, 144–151. [CrossRef]
5. Cheng, C.; Wang, S.; Wu, J.; Yu, Y.; Li, R.; Eda, S.; Chen, J.; Feng, G.; Lawrie, B.; Hu, A. Bisphenol A sensors on polyimide fabricated by laser direct writing for onsite river water monitoring at attomolar concentration. *ACS Appl. Mater. Interfaces* **2016**, *8*, 17784–17792. [CrossRef] [PubMed]
6. Liu, W.; Huang, Y.; Peng, Y.; Walczak, M.; Wang, D.; Chen, Q.; Liu, Z.; Li, L. Stable wearable strain sensors on textiles by direct laser writing of graphene. *ACS Appl. Nano Mater.* **2020**, *3*, 283–293. [CrossRef]
7. Fiodorov, V.; Ratautas, K.; Mockus, Z.; Trusovas, R.; Mikoliūnaitė, L.; Račiukaitis, G. Laser-assisted selective fabrication of copper traces on polymers by electroplating. *Polymers* **2022**, *14*, 781. [CrossRef]
8. Trusovas, R.; Ratautas, K.; Račiukaitis, G.; Niaura, G. Graphene layer formation in pinewood by nanosecond and picosecond laser irradiation. *Appl. Surf. Sci.* **2019**, *471*, 154–161. [CrossRef]
9. Kulyk, B.; Silva, B.F.R.; Carvalho, A.F.; Silvestre, S.; Fernandes, A.J.S.; Martins, R.; Fortunato, E.; Costa, F.M. Laser-induced graphene from paper for mechanical sensing. *ACS Appl. Mater. Interfaces* **2021**, *13*, 10210–10221. [CrossRef]
10. Chyan, Y.; Ye, R.; Li, Y.; Singh, S.P.; Arnusch, C.J.; Tour, J.M. Laser-induced graphene by multiple lasing: Toward electronics on cloth, paper, and food. *ACS Nano* **2018**, *12*, 2176–2183. [CrossRef]
11. Santos, N.F.; Pereira, S.O.; Moreira, A.; Girão, A.V.; Carvalho, A.F.; Fernandes, A.J.S.; Costa, F.M. IR and UV laser-induced graphene: Application as dopamine electrochemical sensors. *Adv. Mater. Technol.* **2021**, *6*, 2100007. [CrossRef]
12. Vivaldi, F.M.; Dallinger, A.; Bonini, A.; Poma, N.; Sembranti, L.; Biagini, D.; Salvo, P.; Greco, F.; Francesco, F.D. Three-dimensional (3D) laser-induced graphene: Structure, properties, and application to chemical sensing. *ACS Appl. Mater. Interfaces* **2021**, *13*, 30245–30260. [CrossRef] [PubMed]
13. Wang, L.; Wang, Z.; Bakhtiyari, A.N.; Zheng, H. A Comparative study of laser-induced graphene by CO_2 infrared laser and 355 nm ultraviolet (UV) laser. *Micromachines* **2020**, *11*, 1094. [CrossRef] [PubMed]
14. Wang, S.; Yu, Y.; Li, R.; Feng, G.; Wu, Z.; Compagnini, G.; Gulino, A.; Feng, Z.; Hu, A. High-performance stacked in-plane supercapacitors and supercapacitor array fabricated by femtosecond laser 3D direct writing on polyimide sheets. *Electrochim. Acta* **2017**, *241*, 153–161. [CrossRef]
15. Peng, Z.; Lin, J.; Ye, R.; Samuel, E.L.G.; Tour, J.M. Flexible and stackable laser-induced graphene supercapacitors. *ACS Appl. Mater. Interfaces* **2015**, *7*, 3414–3419. [CrossRef]
16. Barber, R.; Cameron, S.; Devine, A.; McCombe, A.; Pourshahidi, L.K.; Cundell, J.; Roy, S.; Mathur, A.; Casimero, C.; Papakonstantinou, P.; et al. Laser induced graphene sensors for assessing pH: Application to wound management. *Electrochem. Commun.* **2021**, *123*, 106914. [CrossRef]
17. Ahmad, M.; Cantarella, G.; Angeli, M.A.C.; Madagalam, M.; Ebner, C.; Ciocca, M.; Riaz, R.; Ibba, P.; Petrelli, M.; Merino, I.; et al. 2.4 GHz microstrip patch antenna fabricated by means of laser induced graphitization of a cellulose-based paper substrate. In Proceedings of the 2021 IEEE International Flexible Electronics Technology Conference (IFETC), Columbus, OH, USA, 8–11 August 2021; pp. 44–46. [CrossRef]
18. Wang, H.; Zhao, Z.; Liu, P.; Guo, X. A soft and stretchable electronics using laser-induced graphene on polyimide/PDMS composite substrate. *Npj Flex. Electron.* **2022**, *6*, 26. [CrossRef]
19. Celiešiūtė, R.; Venckus, T.; Vaitekonis, Š.; Pauliukaite, R. Electrosynthesis and characterisation of poly(folic acid) films. *Electrochim. Acta* **2014**, *138*, 62–68. [CrossRef]
20. Younis, I.R.; Stamatakis, M.K.; Callery, P.S.; Meyer-Stout, P.J. Influence of pH on the dissolution of folic acid supplements. *Int. J. Pharm.* **2009**, *367*, 97–102. [CrossRef]
21. Venckus, T.; Celiešiūtė, R.; Radzevič, A.; Rakickas, T.; Vaitekonis, Š.; Ruelė, Ž.; Pauliukaite, R. Application of polyfolates in the development of electrochemical glucose biosensors. *Electroanalysis* **2014**, *26*, 2273–2282. [CrossRef]
22. He, M.; Zheng, X. A highly sensitive and selective method for dopamine detection based on poly(folic acid) film modified electrode. *J. Mol. Liq.* **2012**, *173*, 29–34. [CrossRef]

23. Žutautas, V.; Jelinskas, T.; Pauliukaite, R. A novel sensor for electrochemical pH monitoring based on polyfolate. *J. Electroanal. Chem.* **2022**, *921*, 116668. [CrossRef]
24. Miao, Y.; Chen, J.; Fang, K. New technology for the detection of pH. *J. Biochem. Biophys. Methods* **2005**, *63*, 1–9. [CrossRef]
25. Khan, M.I.; Khan, A.M.; Nouman, A.; Azhar, M.I.; Saleem, M.K. pH sensing materials for MEMS sensors and detection techniques. In Proceedings of the International Conference on Solid-State and Integrated Circuit, Singapore, 17–18 March 2012; IACSIT Press: Singapore, 2012; Volume 32, pp. 18–22.
26. Chinnam, K.C. Capacitive pH-Sensors Using pH Sensitive Polymer. Master's Thesis, Linköping University, Linköping, Sweden, 2009.
27. Abu-Thabit, N.; Hakeem, A.S.; Mezghani, K.; Ratemi, E.; Elzagheid, M.; Umar, Y.; Primartomo, A.; Al Batty, S.; Azad, A.K.; Al Anazi, S.; et al. Preparation of pH-Indicative and flame-retardant nanocomposite films for smart packaging applications. *Sensors* **2020**, *20*, 5462. [CrossRef] [PubMed]
28. Kumar, S.; Bansod, B.S.; Thakur, R.; Jharval, M. Soil pH sensing techniques and technologies—A review. *Int. J. Adv. Res. Electric. Electron. Instrument. Eng.* **2015**, *4*, 4452–4456.
29. Abu-Thabit, N.; Umar, Y.; Ratemi, E.; Ahmad, A.; Abuilaiwi, F.A. A flexible optical pH sensor based on polysulfone membranes coated with pH-responsive polyaniline nanofibers. *Sensors* **2016**, *16*, 986. [CrossRef] [PubMed]
30. Scholz, F. From the Leiden jar to the discovery of the glass electrode by Max Cremer. *J. Solid State Electrochem.* **2011**, *15*, 5–14. [CrossRef]
31. Lange, U.; Roznyatovskaya, N.V.; Mirsky, V.M. Conducting polymers in chemical sensors and arrays. *Anal. Chim. Acta* **2008**, *614*, 1–26. [CrossRef]
32. Brownson, D.A.C.; Kampouris, D.K.; Banks, C.E. Graphene electrochemistry: Fundamental concepts through to prominent applications. *Chem. Soc. Rev.* **2012**, *41*, 6944–6976. [CrossRef]
33. Eng, A.Y.S.; Chua, C.K.; Pumera, M. Intrinsic electrochemical performance and precise control of surface porosity of graphene-modified electrodes using the drop-casting technique. *Electrochem. Commun.* **2015**, *59*, 86–90. [CrossRef]
34. Huang, Q.; Loveridge, M.J.; Genieser, R.; Lain, M.J.; Bhagat, R. Electrochemical evaluation and phase-related impedance studies on silicon–few layer graphene (FLG) composite electrode systems. *Sci. Rep.* **2018**, *8*, 1386. [CrossRef]
35. Pauliukaite, R.; Ghica, M.E.; Fatibello-Filho, O.; Brett, C.M.A. Electrochemical impedance studies of chitosan-modified electrodes for application in electrochemical sensors and biosensors. *Electrochim. Acta* **2010**, *55*, 6239–6247. [CrossRef]
36. Lasia, A. Impedance of porous electrodes. *ECS Trans.* **2008**, *13*, 1–18. [CrossRef]
37. Huang, J.; Gao, Y.; Luo, J.; Wang, S.; Li, C.; Chen, S.; Zhang, J. Editors' Choice—Review—Impedance response of porous electrodes: Theoretical framework, physical models and applications. *J. Electrochem. Soc.* **2020**, *167*, 166503. [CrossRef]
38. Nguyen, T.Q.; Breitkopf, C. Determination of diffusion coefficients using impedance spectroscopy data. *J. Electrochem. Soc.* **2018**, *165*, 826–831. [CrossRef]
39. Žemaitis, A.; Mimidis, A.; Papadopoulos, A.; Gečys, P.; Račiukaitis, G.; Stratakis, E.; Gedvilas, M. Controlling the wettability of stainless steel from highly-hydrophilic to super-hydrophobic by femtosecond laser-induced ripples and nanospikes. *RSC Adv.* **2020**, *62*, 37956–37961. [CrossRef]
40. Agrawal, G.; Negi, Y.S.; Pradhan, S.; Dash, M.; Samal, S.K. Wettability and contact angle of polymeric biomaterials. In *Characterization of Polymeric Biomaterials*; Woodhead Publishing: Sawston, UK, 2017; pp. 57–81. [CrossRef]
41. Hubbe, M.A. Why, after all, are chitosan films hydrophobic? *BioResources* **2019**, *14*, 7630–7631. [CrossRef]
42. Rahimi, R.; Ochoa, M.; Tamayol, A.; Khalili, S.; Khademhosseini, A.; Ziaie, B. Highly stretchable potentiometric pH sensor fabricated via laser carbonization and machining of carbon- polyaniline composite. *ACS Appl. Mater. Interfaces* **2017**, *9*, 9015–9023. [CrossRef]
43. Zhang, L.; Wang, L.; Li, J.; Cui, C.; Zhou, Z.; Wen, L. Surface engineering of laser-induced graphene enables long-term monitoring of on-body uric acid and pH simultaneously. *Nano Lett.* **2022**, *22*, 5451–5458. [CrossRef]
44. Lampinen, A.; See, E.; Emelianov, A.; Myllyperkiö, P.; Johansson, A.; Pettersson, M. Laser-induced tuning of graphene field-effect transistors for pH sensing. *Phys. Chem. Chem. Phys.* **2023**, *25*, 10778–10784. [CrossRef]